

Elsevier Editorial System(tm) for Ecological Modelling
Manuscript Draft

Manuscript Number:

Title: A Hierarchical Analysis of Terrestrial Ecosystem Model Biome-BGC: 1. Equilibrium Analysis and Model Calibration

Article Type: Research Paper

Keywords: Terrestrial Ecosystem; BIOME-BGC; Hierarchical Analysis; Equilibrium Analysis; Model Calibration

Corresponding Author: Research Scientist Weile Wang, Ph.D.

Corresponding Author's Institution:

First Author: Weile Wang, Ph.D.

Order of Authors: Weile Wang, Ph.D.; Kazuhito Ichii; Hirofumi Hashimoto; Andrew R Michaelis; Peter E Thornton; Ramakrishna R Nemani

Abstract: The increasing complexity of ecosystem models represents a major difficulty in calibrating model parameters and analyzing simulated results. To address this problem, this study develops a hierarchical scheme that simplifies the Biome-BGC model into three functionally cascaded tiers and analyzes them sequentially. The first-tier model focuses on leaf-level ecophysiological processes; it simulates evapotranspiration and photosynthesis with prescribed leaf area index (LAI). The restriction on LAI is then lifted in the following two model tiers, which analyze how carbon and nitrogen is cycled at the whole-plant level (the second tier) and in all litter/soil pools (the third tier) to dynamically support the prescribed canopy. In particular, this study analyzes the steady state of these two model tiers by a set of equilibrium equations that are derived from Biome-BGC algorithms and are based on the principle of mass balance. Instead of spinning-up the model for thousands of climate years, these equations are able to estimate carbon/nitrogen stocks and fluxes of the target (steady-state) ecosystem directly from the results obtained by the first-tier model. The model hierarchy is examined with model experiments at four Ameri-Flux sites. The results indicate that the proposed scheme can effectively calibrate Biome-BGC to simulate observed fluxes of evapotranspiration and photosynthesis; and the carbon/nitrogen stocks estimated by the equilibrium analysis

approach are highly consistent with the results of model simulations. Therefore, the scheme developed in this study may serve as a practical guide to calibrate/analyze Biome-BGC; it also provides an efficient way to solve the problem of model spin-up, especially for applications over large regions. The same methodology may help analyze other similar ecosystem models as well.

1 **A Hierarchical Analysis of Terrestrial Ecosystem Model BIOME-BGC:**
2 **I. Equilibrium Analysis and Model Calibration**

3
4
5
6
7
8
9
10
11
12
13
14
15
16
17
18
19
20
21
22
23

Weile Wang ^{1,2}, Kazuhito Ichii ³, Hirofumi Hashimoto ^{1,2}, Andrew R. Michaelis ^{1,2},
Peter E. Thornton ⁴, Ramakrishna R. Nemani ²

- 1) California State University, Monterey Bay, Seaside, CA, USA
- 2) NASA Ames Research Center, Moffett Field, CA, USA
- 3) Faculty of Symbiotic Systems Science, Fukushima University, Japan
- 4) National Center for Atmospheric Research, Boulder, CO, USA

Corresponding Author:
Weile Wang
(c/o Ramakrishna R. Nemani)
Mail Stop 242-4, NASA Ames Research Center, Moffett Field, 94035, USA
Tel: +1-650-604-6444, Fax: +1-650-604-6569
E-mail: weile.wang@gmail.com

Abstract

The increasing complexity of ecosystem models represents a major difficulty in calibrating model parameters and analyzing simulated results. To address this problem, this study develops a hierarchical scheme that simplifies the Biome-BGC model into three functionally cascaded tiers and analyzes them sequentially. The first-tier model focuses on leaf-level ecophysiological processes; it simulates evapotranspiration and photosynthesis with prescribed leaf area index (LAI). The restriction on LAI is then lifted in the following two model tiers, which analyze how carbon and nitrogen is cycled at the whole-plant level (the second tier) and in all litter/soil pools (the third tier) to dynamically support the prescribed canopy. In particular, this study analyzes the steady state of these two model tiers by a set of equilibrium equations that are derived from Biome-BGC algorithms and are based on the principle of mass balance. Instead of spinning-up the model for thousands of climate years, these equations are able to estimate carbon/nitrogen stocks and fluxes of the target (steady-state) ecosystem directly from the results obtained by the first-tier model. The model hierarchy is examined with model experiments at four Ameri-Flux sites. The results indicate that the proposed scheme can effectively calibrate Biome-BGC to simulate observed fluxes of evapotranspiration and photosynthesis; and the carbon/nitrogen stocks estimated by the equilibrium analysis approach are highly consistent with the results of model simulations. Therefore, the scheme developed in this study may serve as a practical guide to calibrate/analyze Biome-BGC; it also provides an efficient way to solve the problem of model spin-up, especially for applications over large regions. The same methodology may help analyze other similar ecosystem models as well.

1. Introduction

The fact that humankind is changing the Earth's climate by polluting the atmosphere with greenhouse gases has generated an imperative for the understanding of, and the ability to simulate, the role terrestrial ecosystems play in the global carbon cycle (IPCC 2007). In response to this call, a variety of biogeochemical ecosystem models have been developed since the 1980s, including CASA (Potter et al. 1993), CENTURY (Parton et al. 1993), TEM (Raich et al. 1991; McGuire et al. 1992), BGC (Running and Coughlan 1988; Running and Hunt 1991), and many others. These models are driven by surface climate variables, and employ algorithms to simulate important ecosystem processes such as the exchange of water between the surface and the atmosphere through evaporation and transpiration, the assimilation and release of carbon through photosynthesis and respiration, and the decomposition of organic matter and the transformation of nitrogen in soil. As such, they provide an important means to simulate regional and global carbon/water cycles, and to assess the impacts of climate variability and its long-term change on these cycles (e.g, Randerson et al. 1997, Cramer et al. 1999, Schimel et al. 2000, Nemani et al. 2003).

Early versions of biogeochemical models usually have simple structures; as models evolve to create more realistic simulations, their later versions become increasingly sophisticated. For example, in Forest-BGC, the first member of the BGC family, leaf area index (LAI) of the vegetation canopy is prescribed, and carbon allocation is solely controlled by external parameters (Running and Coughlan 1988). In the latest BGC model (Biome-BGC, version 4.2), in contrast, LAI is dynamically simulated and updated at daily scales with an integrated consideration of both carbon and nitrogen fluxes

(Thornton et al. 2002). The current Biome-BGC also treats litter and soil processes in much detail, simulating the transformation of carbon and nitrogen between four different litter pools and four different soil pools (Thornton and Rosenbloom 2005; Thornton 1998). (The latest Biome-BGC model and its documentation are available online at <http://www.ntsg.umd.edu>.)

An indicator of a model's complexity may be the number of parameters that are used in the model to characterize various ecosystem processes or to represent different environmental properties. Currently, the core algorithm of Biome-BGC requires 67 parameters to be specified, of which 23 parameters are assumed constant model-wide, 34 parameters are specific to the plant functional type (PFT), and 10 parameters are specific to the study site. Determining appropriate values for these parameters requires great diligence: White et al. (2000) represents 40 pages of referenced source data to calculate a default set of ecophysiological parameters for Biome-BGC (which are supplied with the distribution of the BGC model). Still, these default parameters are intended for general guidance only: for a model as complex as Biome-BGC, small uncertainties in the parameters may propagate to generate a wide range of variability in the subsequent simulations. For particular applications, therefore, model parameters should be calibrated against site-specific measurements to ensure the quality of the experiment results.

Because ecosystem processes tend to be nonlinear, numerical inversion algorithms are usually adopted for parameter calibrations. In general, these algorithms define a cost function that measures the mismatch between model simulations and the corresponding observations, and search for a set of "optimal" parameter values that minimize the cost function. The search process usually starts with examining how the cost function

responds to small changes in the parameters of interest; it then uses this information to determines new parameter values that decrease the cost function. This procedure is repeated until the minimum of the cost function is reached. Applications and reviews of typical inversion algorithms used in ecosystem model calibration can be found, for instance, in Wang et al. (2001, 2006), Knorr and Kattge (2005), Williams et al. (2005), and Raupach et al. (2005).

There are a few difficulties, or limitations, associated with the inversion of complicated models. First, because the search for an optimal solution is an iterative process, the inversion procedure may consume lots of processing power when the model is complicated and there are many parameters to calibrate (Wang et al. 2001, Raupach et al. 2005). Second, deciding the subset of parameters for calibration itself can be a difficult process. With the computation costs considered, generally we would like to calibrate parameters that are important and mutually independent (Harmon and Challenor 1997). However, parameters (and the processes they characterize) in complex models preclude easy determination of the relative importance and independence of their component parts. Finally and most importantly, numerical inversion algorithms treat the ecosystem model as a “black-box” process, in which only the tested relationships between inputs (i.e., changes in parameters) and outputs (i.e., usually a few selected variables for which observations are available) are used. Thus the retrieval of optimal parameter values does not necessarily help with insight into the physical processes represented by the model. There are occasions in which we may be more interested in understanding why and how (rather than knowing what) certain values of parameters

render the most realistic simulations. Numerical algorithms alone cannot fully address these questions.

Altogether, as today's ecosystem models strive to create more realistic simulations, their increasing complexity induces a major difficulty in calibrating parameters and analyzing results, which in turn limits the application of the models themselves. To address this problem, on one hand, simplifications are necessary; on the other hand, the simulation capacity of the models should not be impaired. This creates a dilemma that is faced by anyone seeking to use modern ecosystem models.

Held (2005) discussed a similar dilemma for climate modeling. As suggested by Held (2005), a general solution to problems of this kind relies on the construction of model hierarchies. For instance, suppose there is a set of models that are coherently related to, but less complex than, the model we are working on. By comparing the behavior of the original complex model to that of simpler ones, we can gain understanding of "how the dynamics change as key sources of complexity are added or subtracted" (Held 2005). Also, parameters can be first calibrated on simpler models, and then applied to more complicated systems.

The set of coherently related models (including the original one) that have different levels of complexity forms a "model hierarchy" (Held 2005). For most ecosystem models, such a model hierarchy is not readily available, but may be constructed by sequentially removing certain functional components from the original model. Motivated by this approach, in this study we develop a model hierarchy for Biome-BGC and demonstrate its application in model analysis and parameter calibration at four AmeriFlux sites.

The rest of the paper is structured as follows. Section 2 represents the derivation and formulation of the model hierarchy. The hierarchical scheme is then applied to analyze and calibrate Biome-BGC at four AmeriFlux sites: Section 3 describes the four AmeriFlux sites and the data compilation, and Section 4 discusses the results of the model demonstration. Finally, Section 5 represents the concluding remarks.

2. Methodology

2.1 Derivation of the model hierarchy

With a focus on the carbon cycle, we identify three key functional tiers in Biome-BGC: 1) photosynthesis and evapotranspiration at the leaf level; 2) carbon (and nitrogen) allocation and respiration at the whole-plant level; and 3) carbon/nitrogen cycles in litter/soil pools (Figure 1). To facilitate the discussion, Table 1 lists abbreviations and symbols that are frequently used in the following sections.

Photosynthesis (PSN) and evapotranspiration (ET) are two closely related processes that occur at the leaf level (Fig. 1a). PSN represents the start of the carbon cycle in Biome-BGC, which assimilates atmospheric CO₂ into the ecosystem (measured by gross primary production, GPP); during the same process, water is transpired from the soil to the atmosphere. In Biome-BGC, both processes are calculated on a basis of projected leaf area – indeed, they can be fully calculated if the leaf area of the canopy (represented by leaf area index or LAI) is known. In other words, if we prescribe LAI but remove the rest of carbon/nitrogen cycles from the model, it should still be able to simulate GPP and ET.

Therefore, such a simple land-surface scheme defines the first model in our hierarchy (referred to as the “first-tier” model).

GPP simulated by the first-tier model provides the primary carbon input for the plant-level carbon cycle (Fig. 1b). In particular, GPP less maintenance respiration (MR) represents carbon that is available for allocation, which potentially can be all allocated to different vegetation tissues based on allometric relationships among them (prescribed as model parameters). Accompanying the allocation of carbon, a certain amount of nitrogen must also be allocated to vegetation tissues so that their C:N ratios (prescribed as model parameters) are maintained. Therefore, the actual allocation is not only determined by available carbon, but also regulated by the amount of available nitrogen (mainly N uptake from the soil). Normally, the determination of N uptake involves complicated calculations of soil/litter processes; however, if we are able to estimate N uptake based on a priori knowledge, these soil/litter processes may be ignored. Therefore, by removing soil/litter processes from the original Biome-BGC, the second model is defined in our hierarchy (referenced as the “second-tier” model). Compared with the first-tier model, the second-tier model incorporates carbon/nitrogen cycles at the plant level, so that the growth of vegetation (LAI, in particular) is now dynamically simulated instead of being prescribed.

Finally we examine carbon/nitrogen cycles in litter and soil pools (Fig. 1c). Per Biome-BGC algorithms, dead vegetation tissues (via turnover or whole-plant mortality) are decomposed through a series of stages and at varying rates, which are represented by multiple litter pools and multiple soil pools (although for simplicity, Fig. 1(c) shows only one litter pool and one soil pool, respectively). In general, organic matter flow from fast-

decaying pools (e.g., litter) to slow-decaying pools (e.g., soil), during which a proportion of carbon is released to the atmosphere through heterotrophic respiration (HR). The cycling of nitrogen is a bit more complicated: depending on the C:N ratios of the organic matter and its destined pool, the decomposition process may release surplus nitrogen (mineralization) or may require extra nitrogen (immobilization). Note that the total soil mineral nitrogen may be lower than that potentially demanded by immobilization and vegetation N uptake: in this case, the actual immobilization and the actual uptake will be prorated. Indeed, it is the central task of simulating all soil/litter processes to estimate the balance among nitrogen mineralization, immobilization, and N uptake. Therefore, the last model in our hierarchy (referred to as the “third-tier” model) is defined by incorporating the above described litter/soil processes to the second-tier model. The third-tier model is the original, complete version of Biome-BGC.

2.2 Equilibrium analysis and model simplifications

In most experiments, model state variables need to be first “spun up” into a steady state with respect to the specified climate and ecophysiological conditions (Thornton and Rosenbloom, 2005). Ideally, if we spin up the model using periodic meteorological data that represent the climatology of the site, the resulting state variables will have the same seasonal cycles, and there will be no interannual variability in them. This idealized steady-state represents a “system equilibrium” of the model. Generally it can be approximated by the climatologies (i.e., mean seasonal-cycles) of the model state variables brought by spinup runs.

205 The analysis and calibration of models can be simplified under the assumed system
206 equilibrium. For instance, because the state variables are periodic at system equilibrium,
207 we need to only specify the *mean* LAI cycle in the first-tier model when calibrating it
208 against observed fluxes of ET and GPP. Furthermore, because there is no interannual
209 variability in the state variables, they can be regarded as constant at annual (or longer)
210 time scales. As such, the “slow” ecosystem processes (i.e., carbon allocation, soil
211 decomposition, etc.) in the second-tier and the third-tier models can be easily analyzed
212 with the principle of mass balance (see below).

213 To illustrate, suppose we have calibrated the first-tier model such that it
214 appropriately simulates observed ET and GPP with prescribed LAI. Now consider how to
215 calibrate the second-tier model. Clearly, if we keep model components that are already
216 calibrated in the first-tier model unchanged, but calibrate the other components (that deal
217 with carbon allocation) in a way that they dynamically support a canopy with the same
218 LAI as previously prescribed, the whole second-tier model will be calibrated.

219 We evaluate the above problem by applying the principle of mass balance: because
220 the LAI of the canopy does not change year to year, carbon annually allocated to leaf
221 must be the same as the annual leaf-carbon loss through decay (i.e., turnover or mortality).
222 The latter can be easily estimated because the leaf carbon stock is already known
223 (determined by LAI and SLA, specific leaf area), and the rates of turnover and mortality
224 are prescribed model parameters. The same approach can be extended to determine
225 carbon stocks and fluxes for other plant components, based on their allometric
226 relationships with leaves (all of which are model parameters). Subsequently, all major

carbon (and nitrogen) fluxes in the second-tier model are derived (see the next section for details).

The analysis and calibration of soil/litter processes in the third-tier model can be simplified in the same way as above. Therefore, once the first-tier model is calibrated, the calibration of the second-tier and the third-tier models can be conducted in an analytical fashion, with no numerical inversion techniques involved. This not only simplifies model calibration in terms of computation, but also provides insight into the underlying ecosystem processes and their interactions. For the first-tier model, because its LAI is fixed, its calibration is rather easy and straightforward (see below).

2.3 Formulation of the model hierarchy

This section discusses in detail how to analyze and calibrate the proposed model hierarchy of Biome-BGC. It identifies the parameters for calibration of ET and GPP in the first-tier model and derives mass-balance equations to estimate carbon/nitrogen fluxes in the second-tier and the third-tier models. Yet it is impossible to cover all components of Biome-BGC in this paper. For more detailed discussions of Biome-BGC, we refer the reader to Thornton (1998) and Thornton et al. (2002).

2.3.1 First-tier model

The first-tier model simulates ET and GPP with prescribed LAI. To calibrate the model, we consider the water-cycle component first.

Biome-BGC simulates water fluxes evaporated from the soil surface and vegetation canopy (i.e., intercepted precipitation), transpired by vegetation, and sublimated from the

snowpack. Of these fluxes, sublimation of snow and evaporation of intercepted water occur under certain conditions (i.e., in winter and on rainy days, respectively), which can be relatively easily differentiated in observations. In addition, for well-vegetated sites, evaporation from the soil surface is generally less important than transpiration from canopy. Therefore, the main focus here is how to calibrate the transpiration of soil water by vegetation.

Biome-BGC uses the Penman-Monteith equation to estimate transpiration rate (E , per projected leaf area), which can also be represented as a diffusive process (Sellers et al. 1997):

$$E = g_v \left[e^*(T_s) - e_a \right] \frac{\rho c_p}{\lambda \gamma}, \quad (1)$$

where g_v is the leaf-level conductance for water vapor, $e^*(T_s)$ is the saturation water vapor pressure at leaf temperature T_s , e_a is the water vapor pressure of the ambient air; and ρ , c_p , λ , and γ are constants that represent the density and specific heat of air, the latent heat of evaporation, and the psychrometric constant.

In Eq. (1), leaf water conductance (g_v) is mainly regulated by stomatal conductance (g_s), which is modeled as a product of a maximum value ($g_{s,max}$) and a series of multiplicative regulators (valued between 0 and 1) that respond to incident radiation (R), vapor pressure deficit (VPD), minimum temperature (T_{min}), and soil water potential (Ψ), that is,

$$g_s = m(R) \cdot m(VPD) \cdot m(T_{min}) \cdot m(\Psi) \cdot g_{s,max} \quad (2)$$

where m represents the regulator functions. Approximate g_v with g_s by substituting Eq. (2) into Eq. (1), giving

$$E = m(R)m(VPD)m(T_{\min})m(\Psi)g_{s,\max}\left[e^*(T_s) - e_a\right]\frac{\rho c_p}{\lambda\gamma}. \quad (3)$$

In Eq. (3), ρ , c_p , λ , and γ are physical constants; VPD and T_{\min} are climate variables that are externally determined; and the incident radiation, R , and the vapor pressure difference, $e^*(T_s) - e_a$, are also mainly determined by climate variables. Therefore, an effective way to calibrate E is to adjust the maximum stomatal conductance, $g_{s,\max}$, and another parameter that affects soil water potential (Ψ). For the latter, because variations of Ψ strongly depend on soil water-holding capacity, we choose the effective depth of soil (d_{eff} , also known as the rooting depth) as the second parameter to calibrate.

Next, we consider the photosynthesis component. Biome-BGC estimates the carbon assimilation rate (A , per projected leaf area) by constraining the Farquhar model (Farquhar et al. 1980) with a CO_2 diffusion equation,

$$A = g_c(C_a - C_i), \quad (4)$$

where C_a and C_i represent atmospheric and intracellular CO_2 concentration, respectively; g_c is the leaf-level conductance for CO_2 , which is related to the conductance of water (g_v) by

$$g_c = g_v/1.6. \quad (5)$$

Therefore, photosynthesis is closely related to transpiration, and once g_v is determined, g_c is determined as well.

In Biome-BGC, Eq. (4) is substituted into the Farquhar model to eliminate the unknown variable C_i , so that the assimilation rate A can be solved. For brevity, the Farquhar model is not presented here (but see Farquhar et al. 1980 for detailed discussion). It is sufficient to indicate that A mainly depends on leaf temperature and leaf

nitrogen, which influence the specific activity and the amount of the Rubisco enzyme, respectively (Thornton et al. 2002). Because temperature is a climate variable, we consider how to adjust leaf nitrogen, which is determined by specific leaf area (SLA), the leaf C:N ratio ($C:N_{\text{leaf}}$), and the fraction of leaf nitrogen in the Rubisco enzyme (f_{lnr}). Of these variables, f_{lnr} has the smallest effect on the rest of carbon/nitrogen cycle (see below), and thus it is chosen as the third parameter to calibrate the rate of photosynthesis.

Altogether, for the first-tier model, we choose two parameters, $g_{s,\text{max}}$ and d_{eff} to calibrate the water-cycle component, and choose another parameter, f_{lnr} , to calibrate the photosynthesis component. After these calibrations, the model is expected to simulate observed ET and GPP reasonably well.

2.3.2 Second-tier model

In the second-tier model, we focus on analyzing the plant-level carbon/nitrogen cycles at system equilibrium. First, we consider the question of how much carbon is required to support leaf growth so that maximum LAI does change year to year. (Here the measure of maximum LAI is used because it applies to both deciduous and evergreen forests. For evergreen forests, LAI simulated by Biome-BGC is assumed to be constant, and thus annual maximum LAI is the same as annual mean LAI). Based on the principle of mass balance, carbon allocated to leaves must be balanced by carbon lost via litterfall and mortality, that is,

$$C_{l,\text{alloc}} = (1 + f_{gr}) \cdot (\alpha + \beta) \cdot C_{l,\text{max}}, \quad (6)$$

where $C_{l,\text{alloc}}$ indicates newly allocated leaf carbon; $C_{l,\text{max}}$ denotes leaf carbon corresponding to maximum LAI; α and β represent the annual rates of litterfall and

overall mortality (the total of β_{age} and β_{fire} shown in Table 1), respectively; and f_{gr} indicates the fraction of carbon that is respired during the growth process, which is assumed to be 0.3 in Biome-BGC. Note that Eq. (6) was derived for evergreen forests based on the assumption that leaf carbon is always $C_{l,max}$. For deciduous forests, because trees shed all their leaves every year, the annual total loss of leaf carbon is approximately $C_{l,max}$, that is, the sum of α and β is 1.

Eq. (6) indicates that $C_{l,alloc}$ can be estimated based on $C_{l,max}$. At the same time, according to the allometric allocation scheme assumed in Biome-BGC, carbon allocated to other vegetation compartments is directly or indirectly proportional to $C_{l,alloc}$. For woody species, these compartments include fine root, live/dead stem, and live/dead coarse root, and the corresponding carbon fluxes are:

$$C_{fr,alloc} = \gamma_1 \cdot C_{l,alloc} , \quad (\text{fine roots}) \quad (7a)$$

$$C_{lst,alloc} = \gamma_2 \cdot \gamma_3 \cdot C_{l,alloc} , \quad (\text{live stem}) \quad (7b)$$

$$C_{dst,alloc} = \gamma_2 \cdot (1 - \gamma_3) \cdot C_{l,alloc} , \quad (\text{dead stem}) \quad (7c)$$

$$C_{lcr,alloc} = \gamma_4 \cdot \gamma_2 \cdot \gamma_3 \cdot C_{l,alloc} , \quad (\text{live coarse root}) \quad (7d)$$

$$C_{dcr,alloc} = \gamma_4 \cdot \gamma_2 \cdot (1 - \gamma_3) \cdot C_{l,alloc} , \quad (\text{dead coarse root}) \quad (7e)$$

where γ 's denote allometric parameters (Table 1). Together, the total amount of annually allocated carbon is estimated as:

$$C_{act,alloc} = (1 + \gamma_1 + \gamma_2 + \gamma_2 \gamma_4) \cdot C_{l,alloc} . \quad (8)$$

and the annual growth respiration (GR) is:

$$GR = \frac{f_{gr}}{1 + f_{gr}} \cdot C_{act,alloc} \approx 0.23 \cdot C_{act,alloc} , \quad (9)$$

where a constant value of 0.3 is assumed for the parameter f_{gr} .

As in Eq. (6), we can write carbon balance equations for all the plant compartments described above. Because the newly allocated carbon to these compartments is already known (Eq. 7), these balance relationships can be inverted to estimate their carbon stocks in term of $C_{l,max}$. For live tissues (i.e., fine roots, live stem/coarse root), because they go through similar aging processes (e.g., litterfall or turnover) as leaves, the following relationships can be formulated:

$$C_{fr,max} = \frac{\alpha_l + \beta}{\alpha_{fr} + \beta} \cdot \gamma_1 \cdot C_{l,max}, \quad (\text{fine roots}) \quad (10a)$$

$$C_{lst} = \frac{\alpha_l + \beta}{\alpha_{lst} + \beta} \cdot \gamma_2 \cdot \gamma_3 \cdot C_{l,max}, \quad (\text{live stem}) \quad (10b)$$

$$C_{lcr} = \frac{\alpha_l + \beta}{\alpha_{lcr} + \beta} \cdot \gamma_4 \cdot \gamma_2 \cdot \gamma_3 \cdot C_{l,max}, \quad (\text{live coarse root}) \quad (10c)$$

where α 's represent the rate of litterfall/turnover of the corresponding tissues. For dead woody tissues (i.e., dead stem/coarse root), they gain carbon from the turnover process of their live counterparts, and they lose carbon only when the whole plant dies. The equations to estimate their biomass are thus:

$$C_{dst} = \left[\frac{\alpha_l + \beta}{\beta} \cdot \gamma_2 \cdot (1 - \gamma_3) + \alpha_{lst} \cdot \frac{\alpha_l + \beta}{\alpha_{lst} + \beta} \cdot \gamma_2 \cdot \gamma_3 \right] \cdot C_{l,max}, \quad (\text{dead stem}) \quad (10d)$$

$$C_{dcr} = \left[\frac{\alpha_l + \beta}{\beta} \cdot \gamma_4 \cdot \gamma_2 \cdot (1 - \gamma_3) + \alpha_{lcr} \cdot \frac{\alpha_l + \beta}{\alpha_{lcr} + \beta} \cdot \gamma_4 \cdot \gamma_2 \cdot \gamma_3 \right] \cdot C_{l,max}, \quad (\text{dead coarse root}) \quad (10e)$$

In Biome-BGC, the default litterfall rate of fine roots (α_{fr}) is the same as leaves (α_l), and the turnover rate of live stem (α_{lst}) is the same as live coarse root (α_{lcr}). It thus can be derived from Eq. (10) that:

$$C_{fr,max} = \gamma_1 \cdot C_{l,max} , \quad (\text{fine roots}) \quad (10a')$$

$$C_{lcr} = \gamma_4 \cdot C_{lst} , \quad (\text{live coarse root}) \quad (10c')$$

$$C_{dcr} = \gamma_4 \cdot C_{dst} . \quad (\text{dead coarse root}) \quad (10e')$$

Eq. (10) allows us to estimate carbon stocks for all vegetation compartments. Based on corresponding C:N ratios prescribed in Biome-BGC, their nitrogen content is also determined. On this basis, we can further calculate the annual maintenance respiration (MR) for these components by (Thornton 1998):

$$MR = 0.218 \cdot N \cdot Q_{10}^{(T-20)/10} \quad (11)$$

where N and T indicate the nitrogen content and the temperature of the component, respectively; the Q_{10} factor is assumed to be 2.0 for all components.

Based on the estimated annual GPP (from the first-tier model) and MR (Eq. 11), the amount of carbon that is potentially available for allocation ($C_{pot, alloc}$) can be estimated as,

$$C_{pot, alloc} = GPP - MR \quad (12)$$

On the other hand, the actually allocated carbon, $C_{act, alloc}$, is given by Eq. (8). Per Biome-BGC algorithms, $C_{act, alloc}$ is the same as $C_{pot, alloc}$ only if vegetation growth is not restrained by available nutrients (i.e., mineral nitrogen); otherwise the surplus carbon ($C_{pot, alloc} - C_{act, alloc}$) is removed from the system¹. The difference between $C_{pot, alloc}$ and $C_{act, alloc}$ thus provides a measure by which to evaluate whether/how the simulated

¹ In the original Biome-BGC, the surplus carbon is removed by reducing GPP by the corresponding amount; in this study, however, we revised the model to remove the surplus carbon by increasing the total amount of autotrophic respiration.

vegetation growth is limited by nitrogen availability. This subject will be further discussed in the next section.

2.3.3 Third-tier model

In the third-tier model, we extend the analysis discussed above to carbon/nitrogen cycles in litter and soil pools. Because the decomposition of litter and soil organic matter is generally limited by soil mineral nitrogen, we first discuss how to quantify nitrogen availability.

Per Biome-BGC algorithms, the two main demands for mineral nitrogen are plant uptake and soil immobilization. When soil mineral nitrogen (N_{smin}) cannot meet the total demands from the two components, the actual allocations (i.e., $N_{act,uptk}$ and $N_{act,immb}$) are made proportionally to their potential demands (i.e., $N_{pot,uptk}$ and $N_{pot,immb}$). Therefore, when N_{smin} is limited, the following ratios are the same:

$$f_{pi} = \frac{N_{act,immb}}{N_{pot,immb}} = \frac{N_{act,uptk}}{N_{pot,uptk}} = \frac{N_{smin}}{N_{pot,immb} + N_{pot,uptk}}, \quad (13)$$

where f_{pi} stands for “the fraction of potential immobilization”, a state variable defined in Biome-BGC.

Eq. (13) indicates that f_{pi} can be estimated from nitrogen uptake by vegetation. Indeed, $N_{pot,uptk}$ is directly estimated from $C_{pot, alloc}$ (Eq. 12) based on the C:N ratios of different vegetation compartments. Similarly, the actually allocated nitrogen ($N_{act,alloc}$) can be estimated from $C_{act,alloc}$ (Eq. 8). Finally, to estimate $N_{act,uptk}$ from $N_{act,alloc}$ we need to deduct the portion of nitrogen (N_{trans}) that is retranslocated within the plant. Based on the carbon/nitrogen stocks in different vegetation compartments (estimated in the second-

tier model) and their decay rate, the calculation of N_{trans} is straightforward and therefore neglected here.

Once f_{pi} is known, we are ready to estimate carbon/nitrogen stocks in all four litter pools (and a coarse woody debris pool) and the four soil pools defined in Biome-BGC. To do this, we notice that these pools are linked in a manner that carbon and nitrogen always flow from faster-decaying pools to slower decaying pools, with no loops formed by these flows; in other words, the inflow of a pool is determined only by the outflow of its upstream pools, but not (directly or indirectly) by its downstream pools (a detailed diagram can be found in Thornton and Rosenbloom 2005). Because the most-upstream pools (i.e., plant compartments) are all known, carbon/nitrogen stocks in these soil/litter pools, as well as the fluxes among them, can be sequentially estimated.

To illustrate, we consider the case of the labile litter pool, which is the first litter pool in Biome-BGC. This pool contains the labile portion of the leaf and fine root litter, and a part of newly allocated carbon/nitrogen that enters the pool when the whole plant dies. Therefore, the total inflow to the labile litter pools is:

$$X_{litr1}^{inflow} = p_{lab} \cdot \left[(\alpha_l + \beta_{age}) \cdot X_{l,max} + (\alpha_{fr} + \beta_{age}) \cdot X_{fr,max} \right] + \beta_{age} \cdot 0.5 \cdot X_{act,alloc} \quad (14)$$

where X denotes either “C” (carbon) or “N” (nitrogen) and p_{lab} is a model parameter that represents the labile proportion of leaf and fine root litter. The constant factor (0.5) in the last term of Eq. (14) represents the proportion of allocated carbon and nitrogen that is stored for vegetation growth in the next growing season (Thornton 1998). Note that all variables in Eq. (14) are known.

The outflow of the labile pool is induced by fire and by decomposition, that is,

$$X_{litr1}^{outflow} = (\beta_{fire} + f_{pi} \cdot m_{corr} \cdot k_{litr1}) \cdot X_{litr1} \quad (15)$$

where β_{fire} indicates fire-induced mortality; k_{litr1} is the base decomposition rate of this litter pool (specified by model parameters), while m_{corr} represents the regulation of climate variations on the decomposition rate. The calculation of m_{corr} mainly involves soil temperature and soil moisture, which are determined based on the results of the first-tier model.

At system equilibrium, the inflow of carbon and nitrogen in Eq. (14) must be balanced by the outflow in Eq. (15). Therefore, the only unknown variable in Eq. (15), X_{litr1} , is determined. Subsequently, the components of the outflow [on the right-hand-side of Eq. (15)] can be calculated, which then are used to estimate the heterotrophic respiration (HR), fire emissions (of carbon and nitrogen), and the carbon/nitrogen inflow for the next downstream pool (in this case, it is the fast microbial recycling pool in soil):

In the example above, the mass balance relationship is used twice to estimate the carbon and the nitrogen stocks of the labile litter pool separately. This is because in Biome-BGC the C:N ratios of the litter pools are not fixed but dynamically simulated. For the soil pools, on the other hand, their C:N ratios are prescribed by model parameters. In this case, carbon fluxes and stocks should be estimated first, and then converted to their nitrogen counterparts based on corresponding C:N ratios. Here, it should be noted that the nitrogen inflow estimated based on the carbon inflow may not be the same as that estimated from the outflows from the upstream pools (as in Eq. 14). When the latter is higher than the former, extra nitrogen is diverted into a special soil nitrogen pool (i.e., mineralization); in the opposite situation, nitrogen is taken from the soil nitrogen pool to cover the deficit (i.e., immobilization).

Through processes of mineralization, immobilization, and uptake (by vegetation), most nitrogen that enters into soil/litter pools is recycled within the ecosystem. On the other hand, there are a few nitrogen fluxes that ultimately escape from the system. For Biome-BGC, the most important nitrogen effluxes include fire emission (as suggested by Eq. 15) and nitrogen volatilization, which occurs in the process of mineralization and is proportional to the mineralized nitrogen. (Because soil mineral nitrogen is usually in deficit, nitrogen leaching is generally less important than the two effluxes mentioned above.)

To keep the nitrogen balance of the whole ecosystem, the above nitrogen effluxes must be compensated by influxes of nitrogen that enter the system. In Biome-BGC, these nitrogen influxes include nitrogen deposition and fixation, both of which are specified by model parameters. To close the nitrogen budget, therefore, a simple way is to adjust the rates of nitrogen deposition and fixation so that they are the same as the total effluxes. Alternatively, we can also adjust the size of the nitrogen/carbon pools (or their C:N ratios) so that the resulted effluxes match with the influxes – this can be done following the scheme outlined in the above sections, and thus is not elaborated.

Finally, it should be noted that for the carbon cycle, all effluxes (respiration and fire emissions) are derived from the primary carbon influx, GPP, following the principle of mass balance. Therefore, the carbon balance of the whole ecosystem is automatically ensured.

3. Datasets

We demonstrate the application of the proposed model hierarchy to analyze and calibrate Biome-BGC at two evergreen-needle-forest (ENF) sites and two deciduous-broadleaf-forest (DBF) sites (Table 2): the Metolius (MT) intermediate-aged pine forest in Oregon, the Niwot Ridge (NR) subalpine conifer forest in Colorado, the Morgan Monroe (MM) deciduous forest in Indiana, and the Willow Creek (WC) deciduous forest in Wisconsin. All these sites are part of the AmeriFlux and Fluxnet networks, where fluxes of water and carbon have been systematically measured hourly (or half-hourly) since the late 1990s or early 2000s (e.g., Schmid et al. 2000; Monson et al. 2002; Law et al. 2003; Cook et al. 2004).

For all sites, flux-tower measurements (mainly ET and GPP) between 2000 and 2004 are averaged over 8-day intervals following the procedures in Yang et al. (2006). In particular, we treat missing values as follows: (1) if more than 70% of data were missing in an 8-day period, this period is marked as missing; (2) if a particular time of day was missing in all 8 days, this period is marked as missing; (3) if neither condition 1 nor 2 were met, we fill missing values with the mean from the non-missing days (Falge et al. 2001).

We collected values for site-specific parameters (Table A1) from multiple datasets. Soil properties (i.e., texture and depth) are generated based on the State Soil Geographic Database (STATSGO; Miller and White, 1998), processed by the same methods as in White and Nemani (2004). Elevation is specified based on the HYDRO1K dataset (<http://edc.usgs.gov/products/elevation/gtopo30/hydro/index.html>). Maximum LAI is determined from the MODIS (Moderate Resolution Imaging Spectroradiometer) dataset (Myneni et al. 2002; Yang et al. 2006). At all sites, snow-free surface albedo is assumed

to be 0.2 (Table A1). The total of nitrogen deposition and fixation is set to 0.5 (gN/m²/yr) by default, which is re-calculated during the calibration (see below).

Last, we compile daily meteorological data between 2000 and 2004 as described in Ichii et al. (2007). Daily maximum and minimum temperature are generated from observations at the Climate Prediction Center (CPC) and the National Weather Service Cooperative Observer Program (COOP) climate stations (Jolly et al., 2005). Vapor Pressure Deficit (VPD) is calculated based on daily minimum temperature (Campbell and Norman, 1998). Precipitation is derived from the U.S. daily precipitation analysis of the Climate Prediction Center (<http://www.cpc.ncep.noaa.gov/products/precip/realtime/retro.shtml>). Radiation data are from the Surface Radiation Budget project (SRB, based on Geostationary Operational Environmental Satellite data; Pinker et al., 2002).

4. Results and Discussion

4.1 First-tier model

We demonstrate the calibration of Biome-BGC following the hierarchical scheme described above. The first step is to specify the mean seasonal cycle of LAI in the first-tier model (Fig. 2). This is done based on the results of pre-calibration model experiments. For the ENF sites, because there is little seasonal variability in the simulated vegetation (not shown), LAI at MT and NR is simply assumed as constant (Fig. 2); for the DBF sites, mean LAI cycles obtained from the pre-calibration simulations are used to specify LAI at MM and WC (Fig. 2). For all four sites, the magnitudes of the prescribed LAI cycles are scaled to those indicated by MODIS LAI (Fig. 2; Table A1).

Fig. 2 indicates some discrepancies in the seasonal trajectories between the prescribed (simulated) LAI and MODIS LAI. For instance, MODIS LAI shows considerable seasonal variation at the two ENF sites, which are not simulated by the model; at the two DNF sites, MODIS LAI reaches its peaks in spring and then stays steady during the summer, while the simulated LAI keeps growing through the season until senescence starts (although the growth rate is slowed down in summer) (Fig. 2). These discrepancies reflect limitations and simplifications of the current BGC model. However, because the mechanisms involved in plant phenology and seasonal allocation dynamics are still poorly understood (Waring and Running, 1998), these discrepancies cannot be easily resolved. Therefore, in this study we make no further attempts to address this problem, but assume the prescribed LAI cycles in Fig. 2 are the best results (in terms of LAI simulation) we can get with the current model, and calibrate the model based on this assumption.

We use the standard Levenberg-Marquardt algorithm (Press et al. 1992) to calibrate the three selected parameters (i.e., $g_{s,max}$, d_{eff} , and f_{lnr}) of the first-tier model. This algorithm searches values for these parameters so that the model optimally (in the sense of least squares of errors) simulates the observed ET and GPP. The calibrated parameters (as well as their original values) are shown in Table 3. First of all, the calibration process reduces the values of $g_{s,max}$ almost by half at all sites: while the default value of $g_{s,max}$ is 0.003 (m/s) for ENF and 0.005(m/s) for DBF, the calibrated $g_{s,max}$ is about 0.0015 (m/s) at MT and NR, and is about 0.0025(m/s) at MM and WC (Table 3). Second, the calibrated d_{eff} is significantly increased at MT (from 1.4m to 2.8m) and NR (from 1.0m to 1.4m), but decreased at WC (from ~1.5m to ~0.4m); at MM, d_{eff} is slightly decreased

(from 0.9m to 0.8m; Table 3). Finally, the calibration process made little change to the values of f_{lnr} at most of the sites – except at WC, where it is raised from 0.08 to 0.10 (Table 3).

The results in Table 3 can be easily understood by comparing ET and GPP simulated with original and calibrated parameters, respectively (Fig. 3). Take ET as an example. Before the calibration, the simulated ET (Fig. 3, black dashed lines) has higher magnitudes than observations (Fig. 3, gray solid line) at all sites. At MT and NR, for instance, the observed maximum ET is about 3 mm/day, while the simulated maximum ET reaches 4-5 mm/day. Because these two sites have warm and dry summers, the higher ET dries out soil rapidly in mid-summer, which in turn induces sudden collapse in the simulated ET (Fig. 3a,b). Indeed, the depletion of soil moisture at MT and NR occurs before the observed ET reaches its maximum (Fig. 3a, b), suggesting that the soil-water-storage capacity at these two sites may also be underestimated. At MM and WC, the observed maximum ET is usually below 4 mm/day, while the simulated maximum ET can reach above 6 mm/day (Fig. 3c,d). Yet, although the simulated ET is much higher than observations, no apparent drawdown of soil moisture occurs at MM and WC (Fig. 3c,d), suggesting their soil-water-storage capacity may be overestimated. Fig. 3 also shows that after calibration, ET and GPP simulated with the revised parameters are much more realistic, matching observations in both magnitude and spread (Fig. 3, black solid lines).

After the calibration, annual ET and GPP can be estimated for these sites. In particular, the estimated GPP is about 1.5~1.9 kgC/m²/year (Table 5), which will be discussed in the following section.

558

559 *4.2 Second- and Third-tier models*

560 The focus of the second- and the third-tier models is to derive the carbon and nitrogen
561 balance in the simulated ecosystem so that it can dynamically support a canopy as
562 prescribed in the first-tier model. Compared with the first-tier model, however, these two
563 model tiers are much less constrained by observational data. Therefore, we simply
564 applied the developed methodology to estimate the carbon/nitrogen stocks and fluxes in
565 the two model tiers. The results represented below are thus for demonstration of the
566 methodology rather than rigorous model calibration.

567 The theoretical analysis of the second-tier model indicates that at system
568 equilibrium, carbon stored in other vegetation tissues are related to leaf carbon by simple
569 ratios that are determined by model parameters describing living-tissue turnover, whole-
570 plant mortality, and carbon allometric allocation (Eq. 10). Table 4 lists the value of these
571 parameters for ENF and DBF (Table 4a), and the value of biomass ratios estimated based
572 on them (Table 4b). For both PFTs (plant functional types), the biomass ratios between
573 fine roots and leaves are 1, those between live stems and leaves are significantly below 1
574 (0.08 for ENF and 0.11 for DBF), and those between dead stems and leaves are far above
575 1 (38.8 for ENF and 64.7 for DBF) (Table 4b). Also, biomass of (live/dead) coarse roots
576 are proportional to the corresponding stems, with a ratio of about 0.3 for ENF and about
577 0.23 for DBF (Table 4b).

578 Because the value of biomass ratios depend only on the model parameters listed in
579 Table 4a, they can be verified with model simulations even when the rest of the model is
580 not fully calibrated. Fig. 4 shows time series of stem-to-leaf ratios simulated in model

spinup runs for all sites (the other biomass ratios are constant as listed in Table 4b and therefore not shown). The simulated biomass ratios generally have some oscillatory variability at the beginning of the simulation (Fig. 4), which is mainly induced by the spinup algorithms of Biome-BGC (these algorithms add additional nitrogen to the system to speed up the growth of vegetation; Thornton and Rosenbloom, 2005). As the simulation becomes steady (which often take more than one thousand climate years), biomass ratios simulated for the same PFT (MT and NR for ENF, and MM and WC for DBF, respectively) converge asymptotically towards the theoretically estimated values (Fig. 4, Table 4). At the end of the simulation, the differences between the estimated and the simulated stem-to-leaf ratios are generally less than one percent (1%) of their absolute values. These results confirm that the theoretically estimated values of Table 4 (and the associated formula of Eq. 10) represent good approximations to real biomass ratios.

The biomass ratios in Table 4 provide a convenient way to estimate carbon stocks in different vegetation compartments (Table A2), and carbon fluxes within the simulated plants (Table 5). At MT, for example, annual GPP is estimated at about 1.9 (kgC/m²/year) and MR is about 0.6 (kgC/m²/year); therefore, about 1.3 (kgC/m²/year) of carbon is available for allocation ($C_{pot,alloc}$; Table 5). However, the actually allocated carbon ($C_{act,alloc}$) is independently estimated to be about 0.56 (kgC/m²/year), approximately 43% of $C_{pot,alloc}$ (Table 5). The same $C_{act,alloc}$ -to- $C_{pot,alloc}$ ratio (~43%) is found at NR, and at MM and WC, the corresponding ratios are about 62% (Table 5).

Per Biome-BGC algorithms, inefficient carbon allocation indicates limited nitrogen availability, which is more formally quantified by the state variable f_{pi} (fraction of potential immobilization; Eq. 13). Based on the carbon budget of vegetation (Table 5)

and the associated C:N ratios (Table A3), we estimate the corresponding nitrogen budget and f_{pi} for all sites (Table 6). At MT, for instance, the simulated vegetation would need about 11.8 (gN/m²/yr) of nitrogen ($N_{pot,alloc}$) in order to allocate all its available carbon; however, the amount of nitrogen ($N_{act,alloc}$) it can actually get is about 5.1 (gN/m²/yr), of which 1.5 (gN/m²/yr) is from retranslocation ($N_{retrans}$) and about 3.5 (gN/m²/yr) is uptake from the soil (N_{uprk}) (Table 6). Therefore, f_{pi} (estimated as the ratio between N_{uprk} and $N_{pot,alloc}$) is about 30% (Table 6). Similarly, f_{pi} is estimated about 30% at NR, and about 42% at MM and WC (Table 6), all indicating limited nitrogen availability.

Once f_{pi} is known, we can estimate all the carbon/nitrogen stocks and fluxes in the soil/litter pools. The estimated soil/litter carbon stocks are listed in Table A2. The estimated nitrogen stocks, though not directly shown, can be easily inferred based on the carbon stocks (Table A2) and the C:N ratios (Table A3). Here we focus on the estimated nitrogen fluxes for the rest of the ecosystem (Table 6). As shown, annually mineralized nitrogen is about 15~17 (gN/m²/yr) at NR and MT, and about 29 (gN/m²/yr) at MM and WC; at the same time, the corresponding immobilized nitrogen is about 12~14 (gN/m²/yr) at NR and MT, and about 19 (gN/m²/yr) at MM and WC (Table 6). Therefore, immobilized nitrogen accounts for about 80% of total mineralization at MT and NR (i.e., the ENF sites), and about 60% at IN and WC (i.e., the DBF sites). Most of the remaining mineralized nitrogen is taken up by the plants (Table 6), and only a small proportion of nitrogen is finally released from the system, mainly through volatilization ($N_{loss,vol}$) and fire ($N_{loss,fire}$). As shown in Table 6, the annual loss of nitrogen is about 0.5 (gN/m²/yr) at MT and NR, and about 0.4 (gN/m²/yr) at MM and WC. Because the loss of nitrogen must

be compensated by the input of nitrogen in to the system, the overall rate of nitrogen deposition and fixation (N_{input}) at each site is thus determined (Table 6).

The determination of N_{input} represents the last step in analyzing the second- and the third-tier model. With this information, as well as the parameters calibrated in the first-tier model, we then run the full BGC-Biome model to verify the calibrations and analyses discussed above. Fig. 5 shows the simulated ET, GPP, and LAI, along with the corresponding observations and the results of the first-tier model. As shown, the model-simulated LAI is highly consistent with that was prescribed in the first-tier model (Fig. 5). For instance, the simulated mean LAI is 3.8 at MT, only about 0.2 (or 5%) lower than the expected value; and at NR, the simulated mean LAI is 3.5, the same as the expectation (Fig. 5a,b). The standard deviation of LAI at the two ENF is less than 0.1 (or 3% of its mean value), which confirms the assumption of its stability (Fig. 5a,b). At the two DBF sites, the simulated maximum LAI varies between 5.8 and 6.2, within $\pm 5\%$ of its expected value; its seasonal trajectories also well match the prescribed mean LAI cycles (Fig. 5c,d). The agreement between the simulated and the prescribed LAI also dictates the agreement between the simulated ET and GPP fluxes and the corresponding results of the first-tier model: indeed, the two sets of simulations are almost identical to each other at all four sites (Fig. 5).

We also compare the simulated carbon stocks of every compartment of the ecosystem with those previously estimated (i.e., the results of Table A2). Fig. 6 shows the scatter plots of the carbon stocks at all sites, with the abscissa (x-) and ordinate (y-) coordinates representing theoretical estimates and model simulations, respectively. The comparison indicates good agreement between the two sets of results: for the two ENF

sites, all the plotted points, ranging from 0.01 (kgC/m², in living wood and fast-decaying soil pools) to 16 (kgC/m², in dead wood and slow-decaying soil pools), lie upon or adjacent to the 1-to-1 line (Fig. 6, upper panels). In fact, the estimated carbon stocks captures almost all (>99.95%) the variance of the simulations based on the r^2 statistics of the linear relationship. Almost the same good correspondence is also found for the DBF sites, with the only outliers at the two fast-decaying litter/soil pools (*litr1* and *soil1*), for which the estimates (~0.01 kgC/m²) are lower than simulations (~0.02 kgC/m²) (Fig. 6, bottom panels). Because these two carbon pools are small and are subject to relatively high seasonal variability (not shown), estimation of the annual mean carbon stocks is biased. However, this does not affect the estimation of the effluxes from them, which are constrained by the carbon balance relationship and thus by the influxes from the upstream carbon pools. Therefore, estimation errors of the two compartments do not propagate to the estimates of other soil/litter pools (Fig. 6).

4.3 Discussions

The above model experiments at the four AmeriFlux sites highlight several major advantages of the proposed hierarchical analysis scheme. First, it notably eases difficulties associated with calibrating an ecosystem model as complicated as Biome-BGC. For instance, by prescribing LAI in the first-tier model, the simulation of daily ET and GPP can be effectively calibrated by adjusting parameters of maximum stomatal conductance, soil effective depth, and fraction of leaf nitrogen in Rubisco.

The analysis of the remaining carbon/nitrogen cycling is also much simplified. In particular, the steady-state of the second- and the third-tier models can be easily

estimated following the derived procedures. For instance, on an annual basis, the biomass of other vegetation components is related to leaf carbon by simple ratios that are totally determined by model parameters. These ratios, along with other derived relationships, provide an efficient way to estimate carbon/nitrogen stocks and fluxes in the simulated ecosystem. Note that this is done without running the model for thousands of climate years to reach its steady state. Therefore, these relationships may provide an alternative method, in addition to those discussed in Thornton and Rosenbloom (2005), to solve the problem of model spinup. They can also be utilized to verify model parameterization when good observational data are available.

However, the analysis of the second- and the third-tier model in this study is solely based on the equilibrium assumption. The derived relationships or the associated results are thus restricted to steady-state ecosystems. For non-steady ecosystems, such as young forests or forests that have undergone recent disturbances, this equilibrium analysis approach alone is insufficient, and the dynamic characteristics of the model around the equilibrium must be taken into account (Thornton et al. 2002). Dynamical analysis of ecosystem models can also be conducted under the proposed hierarchical model scheme, which we expect to address in future studies.

5. Conclusions

This study develops a hierarchical scheme to analyze and calibrate the terrestrial ecosystem model Biome-BGC. Under this scheme, Biome-BGC is divided into three functionally cascaded tiers. The first-tier model focuses on ecophysiological processes at the leaf level. It allows LAI in the model to be specified based on *a priori* information

(usually observations), and simulates observed evapotranspiration and photosynthesis with the prescribed LAI. The restriction on prescribed LAI is then lifted in the following two tiers, which analyze how carbon and nitrogen is cycled in the simulated ecosystem to dynamically support the prescribed canopy. In particular, the second-tier model considers the cycling of carbon at the whole-plant level. Based on the principle of carbon balance, it estimates biomass storage in all vegetation components and their demands for annual carbon allocation directly from the prescribed (and thus observed) LAI and the allometric allocation relationships described in Biome-BGC. By comparing carbon that is potentially available for allocation with carbon that is actually allocated, this tier of the model also evaluates how vegetation carbon allocation is limited by soil nitrogen availability. The third-tier model extends the methodology of the second tier to analyze carbon/nitrogen stocks and fluxes in all litter/soil pools. It calculates nitrogen fluxes of mineralization and immobilization resulting from the decomposition of soil organic matter and litter biomass. It also estimates nitrogen fluxes that are escaped from the ecosystem during these processes, and finally, determines how much nitrogen must be input annually to meet the total nitrogen balance of the simulated ecosystem.

This model hierarchy is examined with model experiments at four AmeriFlux sites. The results indicate that this approach simplifies the calibration of Biome-BGC, and also helps to diagnose the internal status of the model, which is difficult by conventional calibration algorithms. In addition, the results indicate good agreement between carbon/nitrogen stocks estimated by the derived methods and those by model simulations, suggesting they may find applications in solving the problem of model spin-up, especially for applications over large regions. However, because these methods are

derived based on the assumption of equilibrium, they cannot directly be applied to analyze non-steady ecosystems. Future efforts are needed to analyze the dynamic characteristics of the model under the proposed hierarchical scheme.

Finally, although this paper mainly focuses on analyzing Biome-BGC, the general concept and methodology developed in this study may help analyze other similar ecosystem models as well.

Acknowledgements

This research was supported by funding from NASA's Science Mission Directorate through EOS. Flux tower measurements were funded by the Department of Energy, the National Oceanic and Atmospheric Administration, the National Space Agency (NASA) and the National Science Foundation. Special thanks to all the scientists and support staff at the flux towers. Jennifer Dungan provided useful feedback on an earlier version of this manuscript.

733 **Appendix: Supplemental Tables**

734 Table A1. Additional site-specific parameters used in the analysis

735

736 Table A2. Estimated carbon stocks in ecosystem compartments (Unit: kgC/m²)

737

738 Table A3. C:N ratios of ecosystem compartments

References

- Campbell G.S. and J.M. Norman, 1998. An introduction to environmental biophysics. Springer-Verlag, pp. 286.
- Cook, B.D., K.J. Davis, W. Wang, A.R. Desai, B.W. Berger, and et al., 2004. Carbon exchange and venting anomalies in an upland deciduous forest in northern Wisconsin, USA, *Agricultural and Forest Meteorology*, **126**, 271-295.
- Cramer, W., D.W. Kicklighter, A. Bondeau, B. Moore III, G. Churkina and et al., 1999. Comparing global models of terrestrial net primary productivity (NPP): overview and key results. *Global Change Biology*, **5**, 1-15.
- Falge, E., D. Baldocchi, R. Olsonb, P. Anthonic, M. Aubinetd, and et al., 2001. Gap filling strategies for long term energy flux data sets. *Agricultural and Forest Meteorology*, **107**, 71–77.
- Farquhar, G.D., S. von Caemmerer, and J.A. Berry, 1980. A biochemical model of photosynthetic CO₂ assimilation in leaves of C₃ species. *Planta*, **149**, 78-90.
- Harmon, R. and P. Challenor, 1997. A Markov chain Monte Carlo method for estimation and assimilation into models. *Ecological Modelling*, **101**, 41-59.
- Held, I.M., 2005. The gap between simulation and understanding in climate modeling. *Bulletin of American Meteorological Society*, **86**, 1609-1614.
- Ichii, K., W. Wang, H. Hashimoto, F. Yang, P. Votava, A.R. Michaelis and R.R. Nemani, 2007, Refinement of rooting depths using satellite-based evapotranspiration seasonality and ecosystem modeling in California. *Remote Sensing of Environment*, (in review).

761 IPCC, 2007. Climate Change 2007: The Physical Science Basis: Contribution of
 762 Working Group I to the Fourth Assessment Report of the Intergovernmental Panel on
 763 Climate Change [Solomon, S., D. Qin, M. Manning, Z. Chen, M. Marquis, K.B.
 764 Averyt, M. Tignor and H.L. Miller (eds.)]. Cambridge University Press, 996 pp.
 765 Jolly, W.M., J.M. Graham, A. Michaelis, R.R. Nemani, and S.W. Running, 2005. A
 766 flexible, integrated system for generating meteorological surfaces derived from point
 767 sources across multiple geographic scales. *Environmental Modeling and Software*, **20**,
 768 873-882.
 769 Knorr, W., and J. Kattge, 2005. Inversion of terrestrial ecosystem model parameter values
 770 against eddy covariance measurements by Monte Carlo sampling. *Global Change*
 771 *Biology*, **11**, 1333-1351.
 772 Law, B.E., O.J. Sun, J. Campbell, S. van Tuyl, and P.E. Thornton, 2003. Changes in
 773 carbon storage and fluxes in a chronosequence of ponderosa pine. *Global Change*
 774 *Biology*, **9**, 510-524.
 775 McGuire, A.D., J.M. Melillo, L.A. Joyce, D.W. Kicklighter, A.L. Grace, and et al., 1992.
 776 Interactions between carbon and nitrogen dynamics in estimating net primary
 777 productivity for potential vegetation in North America. *Global Biogeochemical*
 778 *Cycles*, **6**, 101-124.
 779 Miller D.A. and R.A. White, 1998. A conterminous United States multilayer soil
 780 characteristics data set for regional climate and hydrology modeling. *Earth*
 781 *Interactions*, **2**, No. 2, 1-13.

782 Monson, R.K., A.A. Turnipseed, J.P. Sparks, P.C. Harley, L.E. Scott-Denton, K.L.
783 Sparks, and T.E. Huxman, 2002. Carbon sequestration in a high-elevation, subalpine
784 forest. *Global Change Biology*, **8**, 459-478.

785 Myneni R.B., S. Hoffman, Y. Knyazikhim, J.L. Privette, J. Glassy, and et al., 2002.
786 Global products of vegetation leaf area and fraction absorbed PAR from year one of
787 MODIS data. *Remote Sensing of Environment*, **83**, 214-231.

788 Nemani, R.R., C.D. Keeling, H. Hashimoto, and et al., 2003. Climate-driven increases in
789 global terrestrial net primary production from 1982 to 1999. *Science*, **300**, 1560-1563.

790 Parton, W.J., J.M.O. Scurlock, D.S. Ojima, T.G. Gilmanov, R.J. Scholes, and et al., 1993.
791 Observations and modeling of biomass and soil organic matter dynamics for the
792 grassland biome worldwide. *Global Biogeochemical Cycles*, **7**, 785-809.

793 Pinker R.T., O. Laszlo, J.D. Tarpley, K. Mitchell, 2002. Geostationary satellite
794 parameters for surface energy balance. *Advances in Space Research*, **30**, 2427-2432.

795 Potter, C. S., J.T. Randerson, C.B. Field, P.A. Matson, P.M. Vitousek, and et al., 1993.
796 Terrestrial ecosystem production: A process model based on global satellite and
797 surface data. *Global Biogeochemical Cycles*, **7**, 811-841.

798 Press, W.H., S.A. Teukolsky, W.T. Vetterling, B.P. Flannery, 1992. Numerical recipes:
799 the art of scientific computing (2nd Ed.), Cambridge University Press, 994 pp.

800 Raich, J.W., E.B. Rastetter, J.M. Melillo, D.W. Kicklighter, P.A. Steudler, and et al.,
801 1991. Potential net primary productivity in South America: application of a global
802 model. *Ecological Applications*, **1**, 399-429.

803 Randerson, J.T., M.V. Thompson, T.J. Conway, I.Y. Fung, and C.B. Field, 1997. The
 804 contribution of terrestrial sources and sinks to trends in the seasonal cycle of
 805 atmospheric carbon dioxide. *Global Biogeochemical Cycles*, **11**, 535-560.

806 Raupach, M.R., P.J. Rayner, D.J. Barrett, R.S. Defries, M. Heimann, D.S. Ojima, S.
 807 Quegan, and C.C. Schmullius, 2005. Model-data synthesis in terrestrial carbon
 808 observation: methods, data requirements and data uncertainty specifications. *Global*
 809 *Change Biology*, **11**, 378-397.

810 Running, S.W. and J.C. Coughlan, 1988. A general model of forest ecosystem processes
 811 for regional applications: I. Hydrologic balance, canopy gas exchange and primary
 812 production processes. *Ecol. Model.*, **42**, 125-154.

813 Running, S.W. and S.T. Gower, 1991. Forest-BGC, a general model of forest ecosystem
 814 processes for regional applications: II. Dynamic carbon allocation and nitrogen
 815 budgets. *Tree Physiology*, **9**, 147-160.

816 Sellers, P.J., R.E. Dickinson, D.A. Randall, and et al., 1997. Modeling the exchanges of
 817 energy, water, and carbon between continents and the atmosphere, *Science*, **275**, 502-
 818 509.

819 Schimel, D., J. Melillo, H. Tian, A.D. McGuire, D. Kicklighter, and et al., 2000.
 820 Contribution of increasing CO₂ and climate to carbon storage by ecosystems of the
 821 United States. *Science*, **287**, 2004-2006.

822 Schmid, H.P., C.S.B. Grimmond, F. Cropley, B. Offerle, and H.-B. Su, 2000.
 823 Measurements of CO₂ and energy fluxes over a mixed hardwood forest in the
 824 Midwestern United States. *Agricultural and Forest Meteorol.*, **103**, 355-373.

825 Thornton, P.E., 1998. Description of a numerical simulation model for predicting the
826 dynamics of energy, water, carbon, and nitrogen in a terrestrial ecosystem. Ph.D.
827 dissertation, University of Montana, Missoula, MT, 280 pp. [Available from
828 Mansfield Library, University of Montana, Missoula, MT 59812.]

829 Thornton, P.E., B.E. Law, H.L. Gholz, K.L. Clark, E. Falge, and et al. 2002. Modeling
830 and measuring the effects of disturbance history and climate on carbon and water
831 budgets in evergreen needleleaf forests. *Agricultural and Forest Meteorology*, **113**,
832 185-222.

833 Thornton, P.E., and N.A. Rosenbloom, 2005. Ecosystem model spin-up: Estimating
834 steady state conditions in a coupled terrestrial carbon and nitrogen cycle model.
835 *Ecological Modelling*, **189**, 25-48.

836 Wang, Y-P, R. Leuning, H.A. Cleugh, and P.A. Coppin, 2001. Parameter estimation in
837 surface exchange models using nonlinear inversion: how many parameters can we
838 estimate and which measurements are most useful? *Global Change Biology*, **7**, 495-
839 510.

840 Wang, Y-P, D. Baldocchi, R. Leuning, E. Falge, and T. Vesala, 2006. Estimating
841 parameters in a land-surface model by applying nonlinear inversion to eddy
842 covariance flux measurements from eight FLUXNET sites. *Global Change Biology*,
843 **12**, 1-19.

844 Waring, R.H. and S.W. Running, 1998. Forest ecosystems: analysis at multiple scales
845 (2nd Ed.). Academic Press, 370 pp.

846 White, M.A., P.E. Thornton, S.W. Running, and R.R. Nemani, 2000. Parameterization
847 and sensitivity analysis of the Biome-BGC terrestrial ecosystem model: net primary
848 production controls. *Earth Interactions*, **4**, No.3, 1-85.

849 White, M.A. and R.R. Nemani, 2004. Soil water forecasting in the continental United
850 States: relative forcing by meteorology versus leaf area index and the effects of
851 meteorological forecast errors. *Canadian Journal of Remote Sensing*, **30**, 717-730.

852 Williams, M. P.A. Schwarz, B.E. Law, J. Irvine, and M.R., Kurpius, 2005. An improved
853 analysis of forest carbon dynamics using data assimilation. *Global Change Biology*,
854 **11**, 89-105.

855 Yang, F., M.A. White, A. Michaelis, K. Ichii, H. Hashimoto, and et al., 2006. Prediction
856 of continental scale evapotranspiration by combining MODIS and AmeriFlux data
857 through Support Vector Machine. *IEEE Transactions on Geoscience and Remote
858 Sensing*, **44**, 3452-3461.

859 Yang, W., D. Huang, B. Tan, J.C. Stoeve, N. Shabanov, and et al., 2006. Analysis of leaf
860 area index and fraction of PAR absorbed by vegetation products from the Terra
861 MODIS sensor: 2000-2005, *IEEE Transactions on Geoscience and Remote Sensing*,
862 **44**, 1829-1842.

Figure Legends

Fig. 1. Schematic diagrams of the proposed hierarchy of Biome-BGC. The three tiers respectively describe (a) photosynthesis (PSN) and evapotranspiration (ET) at leaf level; (b) carbon and nitrogen cycles at whole-plant level, and (c) carbon and nitrogen cycles in soil and litter pools. Symbols and abbreviations are explained in Table 1.

Fig. 2. Mean LAI cycles prescribed in the first-tier model (dark lines). The gray lines indicate mean MODIS LAI cycles.

Fig. 3. ET and GPP simulated by the first-tier model with original parameters (dotted black lines; “ORI”) and calibrated parameters (solid black lines; “CAL”). The gray lines (“OBS”) show the corresponding tower measurements.

Fig. 4. Evolutions of biomass ratios in model “spin-up” simulations for (a) Evergreen Needle Forest and (b) Deciduous Broadleaf Forest. The two panels (from top to bottom) show biomass ratios between: (1) live stems and leaves; (2) dead stems and leaves, respectively.

Fig. 5. ET, GPP, and LAI simulated by the calibrated Biome-BGC model (solid black lines; “BGC”). Also shown are the corresponding results of the first-tier model (dotted black lines; “BGC-T1”) and the tower measurements (solid gray lines; “OBS”).

886 Fig. 6. Comparison between carbon stocks estimated by the hierarchical analysis (of the
887 second- and the third-tier models) and simulated by the calibrated Biome-BGC model.

Tables

Table 1. List of frequently used abbreviations (a), and symbols for state variables (b) and ecosystem compartments (c).

(a) General abbreviations

Abbreviation	Description
PSN	Photosynthesis
GPP	Gross Primary Production
NPP	Net Primary Production
NEE	Net Ecosystem Exchange
MR	Maintenance Respiration
GR	Growth Respiration
AR	Autotrophic Respiration
HR	Heterotrophic Respiration
PFT	Plant Functional Type
ENF	Evergreen Needle-leaf Forest
DBF	Deciduous Broadleaf Forest
LAI	Leaf Area Index
SLA	Specific Leaf Area

(b) State Variables

Symbol	Units	Description
α_{lf}	1/yr	annual leaf and fine root turnover fraction
α_{wd}	1/yr	annual live wood turnover fraction
β_{age}	1/yr	annual whole-plant mortality fraction
β_{fire}	1/yr	annual fire mortality fraction
γ_1	(0~1)	allocation ratio – new fine root C : new leaf C
γ_2	(0~1)	allocation ratio – new stem C : new leaf C
γ_3	(0~1)	allocation ratio – new live wood C : new total wood C
γ_4	(0~1)	allocation ratio – new coarse root C : new stem C
d_{eff}	m	effective soil depth
f_{lnr}	(0~1)	fraction of leaf nitrogen in Rubisco
f_{pi}	(0~1)	fraction of actual immobilization (of soil mineral nitrogen) to potential immobilization
$g_{s,max}$	ms ⁻¹	maximum stomatal conductance
C_x	kgC/m ²	carbon stock or carbon flux specified by the subscript
	kgC/m ² /s	
N_x	gC/m ²	nitrogen stock or nitrogen flux specified by the subscript
	gC/m ² /s	
$C:N_x$	ratio	carbon-nitrogen mass ratio

898 (c) Ecosystem Compartments

899

Symbol	Ecosystem Compartment
<i>lf</i>	leaf
<i>fr</i>	fine root
<i>lst</i>	live stem
<i>dst</i>	dead stem
<i>lcr</i>	live coarse root
<i>dcr</i>	dead coarse root
<i>cwd</i>	coarse woody debris
<i>litr1</i>	litter – labile proportion
<i>litr2</i>	litter – unshielded cellulose proportion
<i>litr3</i>	litter – shielded cellulose proportion
<i>litr4</i>	litter – lignin proportion
<i>soil1</i>	soil – Fast microbial recycling proportion
<i>soil2</i>	soil – Medium microbial recycling proportion
<i>soil3</i>	soil – Slow microbial recycling proportion
<i>soil4</i>	soil – Recalcitrant (slowest) proportion

900 Table 2. Site Descriptions

901

Site (symbol)	Location	Veg. type*	Period	References
Metolius-intermediate aged forest, OR (MT)	44.45, -121.56	ENF	2002-2004	Law et al. (2003)
Nitwot Ridge, CO (NR)	40.03, -105.55	ENF	2000-2004	Monson et al. (2002)
Morgan Monroe state forest, IN (MM)	39.32, -86.41	DBF	2000-2004	Schmid et al. (2000)
Willow Creek, WI (WC)	45.91, -90.08	DBF	2000-2004	Cook et al. (2004)

902

903 * ENF, evergreen needleleaf forest; DBF, deciduous broadleaf forest.

Table 3. Site-specific parameters calibrated in the first-tier model.

	MT	NR	MM	WC
$g_{s,max} (\times 100)$	0.16 (0.30)	0.14 (0.30)	0.27 (0.50)	0.25 (0.50)
d_{eff}	2.81 (1.44)	1.43 (1.04)	0.83 (0.93)	0.40 (1.52)
f_{lnr}	0.06	0.06	0.08	0.10 (0.08)

Bracketed numbers indicate original values of the corresponding parameters (if they are changed by the calibration process).

909 Table 4. (a) Parameters of vegetation turnover, mortality, and allocation, and estimated (b)
 910 biomass ratios between different vegetation compartments

911

912 (a) Parameters of vegetation turnover, mortality, and allocation

	ENF (MT, NR)	DBF (MM, WC)
α_{lf}	0.25	1.0
α_{wd}	0.70	0.70
β_{age}	0.005	0.01
β_{fire}	0.01	0.0025
γ_1	1	1
γ_2	2.2	0.8
γ_3	0.1	0.1
γ_4	0.3	0.23

913

914 (b) Biomass ratios between different vegetation compartments

	ENF (MT, NR)	DBF (MM, WC)
$C_{fr} : C_{lf}$	1	1
$C_{lst} : C_{lf}$	0.08	0.11
$C_{dst} : C_{lf}$	38.8	64.7
$C_{lcr} : C_{lst}$	0.3	0.23
$C_{dcr} : C_{dst}$	0.3	0.23

915 Table 5. Carbon fluxes (units: kgC/m²/year) estimated in the second-tier model
 916

	MT	NR	MM	WC
GPP	1.91	1.51	1.81	1.56
MR	0.60	0.37	0.54	0.30
$C_{pot,alloc}$	1.31	1.14	1.26	1.26
$C_{act,alloc}$	0.56	0.49	0.78	0.79
$C_{act,alloc} / C_{pot,alloc}$	0.43	0.43	0.62	0.63

917 Table 6. Nitrogen fluxes (units: gN/m²/year) and f_{pi} estimated in the third-tier model.
918

	MT	NR	MM	WC
$N_{pot,alloc}$	11.8	10.3	22.6	22.6
$N_{act,alloc}$	5.1	4.4	14	14
$N_{retrans}$	1.5	1.4	4.6	4.6
N_{uptk}	3.5	3.1	9.6	9.6
f_{pi}	30%	30%	42%	42%
N_{min}	17.2	14.6	28.7	28.6
N_{immob}	14.1	11.9	19.2	19.1
$N_{loss,vol}$	0.17	0.15	0.29	0.29
$N_{loss,fire}$	0.37	0.37	0.10	0.10
N_{input}	0.54	0.52	0.39	0.39

919 Table A1. Additional site-specific parameters used in the analysis
 920

	MT	NR	MM	WC
Elevation	915	3105	261	479
Latitude	44.45	40.03	39.32	45.91
Sand (%)	61	59	27	33
Clay (%)	29	31	58	33
Silt (%)	10	10	15	34
Albedo (snow-free)	0.2	0.2	0.2	0.2
Maximum LAI*	4.0	3.5	6	6

921
 922 * LAI is *not* a standard Biome-BGC parameter. Values shown here are based on MODIS
 923 measurements.

924 Table A2. Estimated carbon stocks in ecosystem compartments (Unit: kgC/m²)
 925

	MT	NR	MM	WC
<i>lf</i>	0.33	0.29	0.20	0.20
<i>fr</i>	0.33	0.29	0.20	0.20
<i>lst</i>	0.03	0.02	0.02	0.02
<i>dst</i>	12.9	11.3	12.9	12.9
<i>lcr</i>	0.008	0.007	0.005	0.005
<i>dcr</i>	3.88	3.39	2.98	2.98
<i>cwd</i>	4.30	5.32	1.36	2.56
<i>litr1</i>	0.01	0.01	0.005	0.01
<i>litr2</i>	0.36	0.45	0.11	0.20
<i>litr3</i>	0.18	0.22	0.05	0.10
<i>litr4</i>	0.67	0.82	0.22	0.41
<i>soil1</i>	0.01	0.01	0.01	0.02
<i>soil2</i>	0.19	0.23	0.11	0.20
<i>soil3</i>	1.91	2.34	1.05	1.97
<i>soil4</i>	12.01	14.75	6.60	12.42

Table A3. C:N ratios of ecosystem compartments*

	ENF (MT, NR)	DBF (MM, WC)
$C:N_{lf}$	42	24
$C:N_{lf,dead}$	93	49
$C:N_{fr}$	42	42
$C:N_{lst}, C:N_{lcr}$	50	50
$C:N_{dst}, C:N_{dcr}$	729	442
$C:N_{cwd}$	721	437
$C:N_{litr1}$	59	46
$C:N_{litr2}$	153	75
$C:N_{litr3}$	56	42
$C:N_{litr4}$	114	65
$C:N_{soil1}$	12	12
$C:N_{soil2}$	12	12
$C:N_{soil3}$	10	10
$C:N_{soil4}$	10	10

* C:N ratios of vegetation and soil pools are prescribed model parameters, while C:N ratios of litter and CWD pools are not prescribed but estimated using algorithms discussed in the text.

Figures

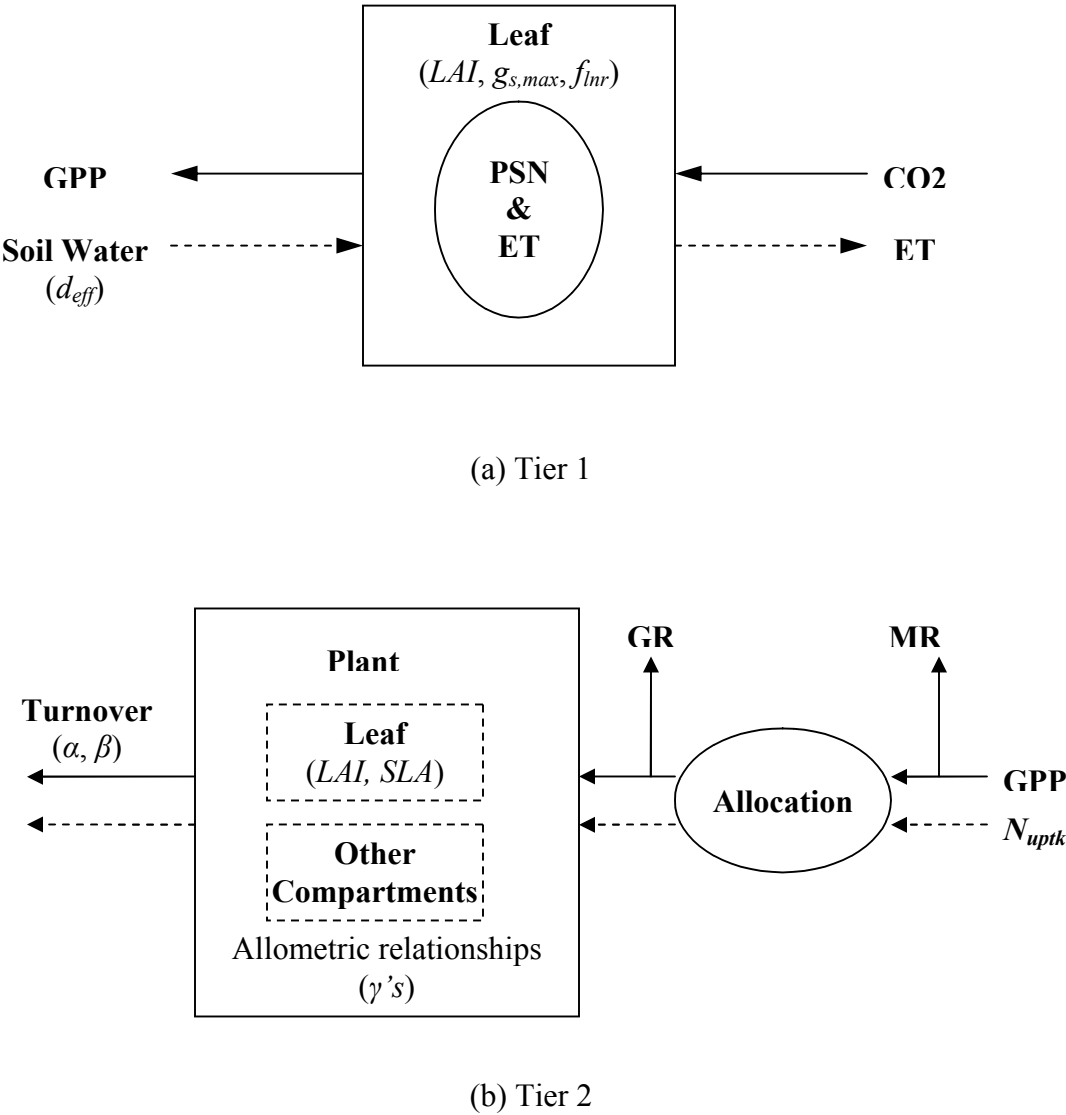
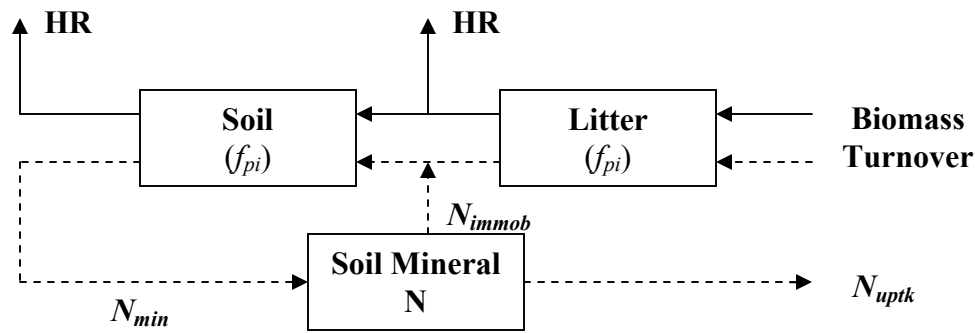


Fig. 1. Schematic diagrams of the proposed hierarchy of Biome-BGC. The three tiers respectively describe (a) photosynthesis (PSN) and evapotranspiration (ET) at leaf level; (b) carbon and nitrogen cycles at whole-plant level, and (c) carbon and nitrogen cycles in soil and litter pools. Symbols and abbreviations are explained in Table 1.



(c) Tier 3

Fig. 1. (continued.)

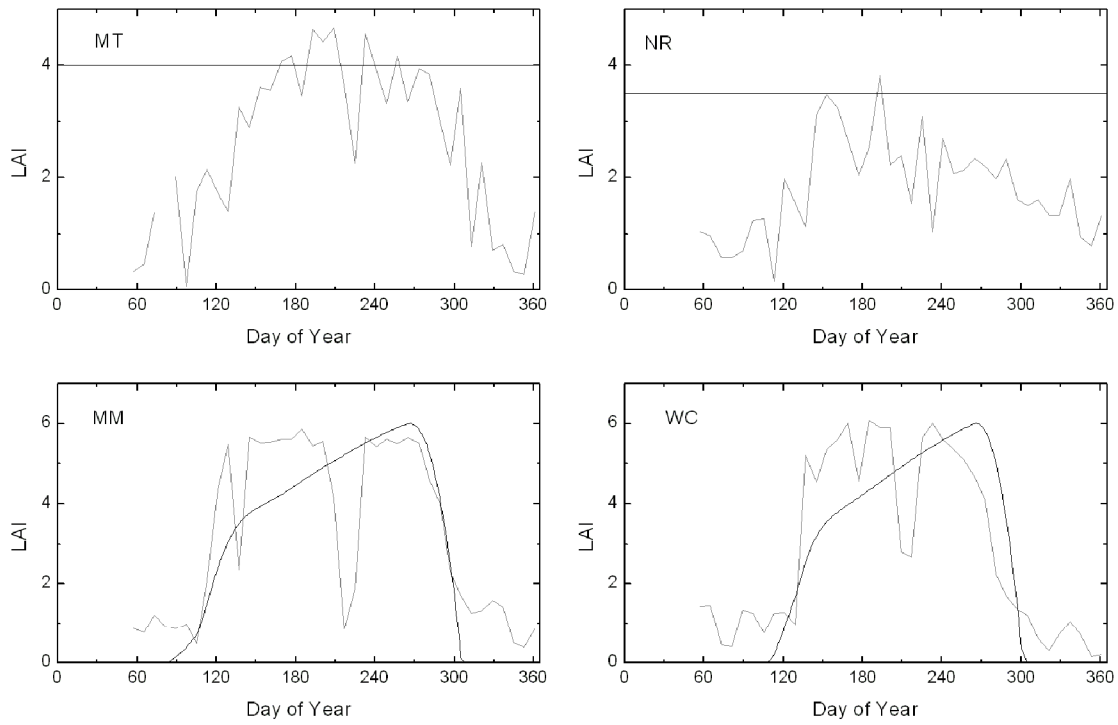
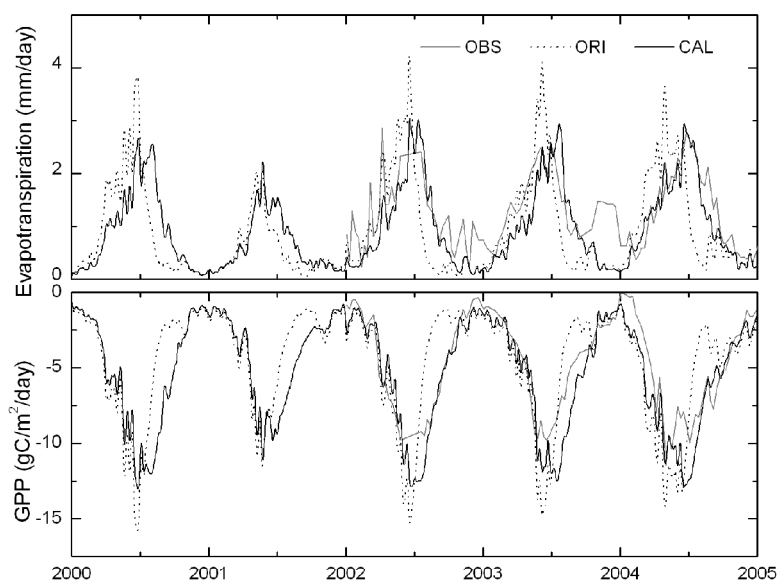
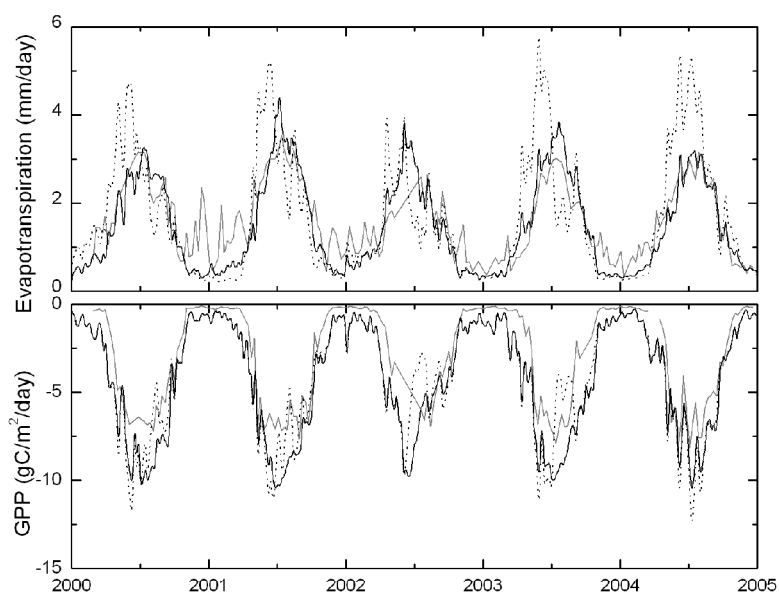


Fig. 2. Mean LAI cycles prescribed in the first-tier model (dark lines). The gray lines indicate mean MODIS LAI cycles.

958



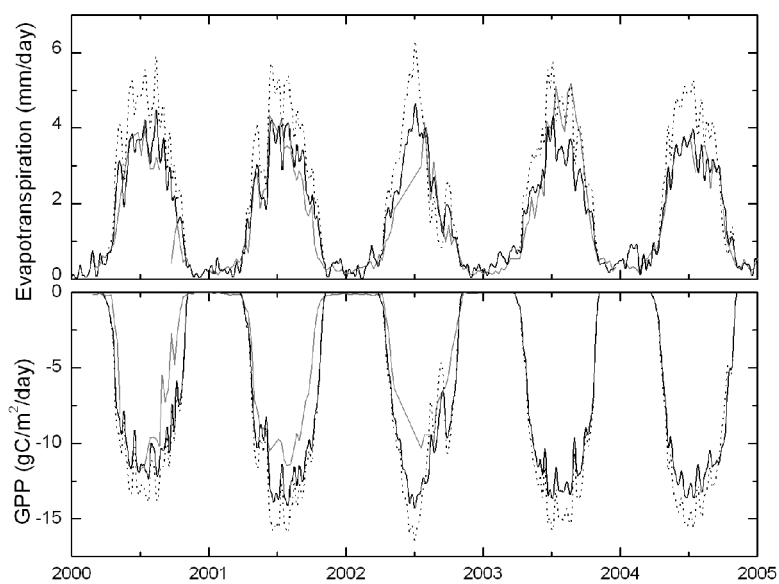
(a) MT



(b) NR

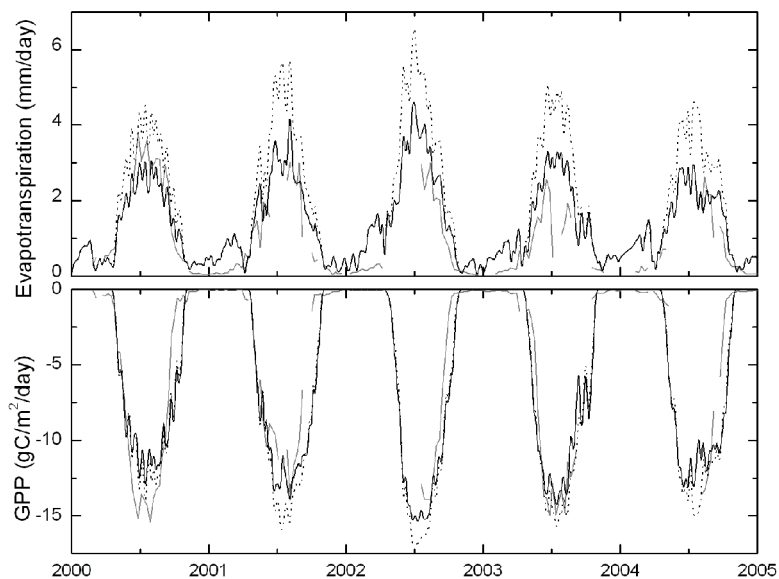
Fig. 3. ET and GPP simulated by the first-tier model with original parameters (dotted black lines; “ORI”) and calibrated parameters (solid black lines; “CAL”). The gray lines (“OBS”) show the corresponding tower measurements.

968



969
970
971

(c) MM

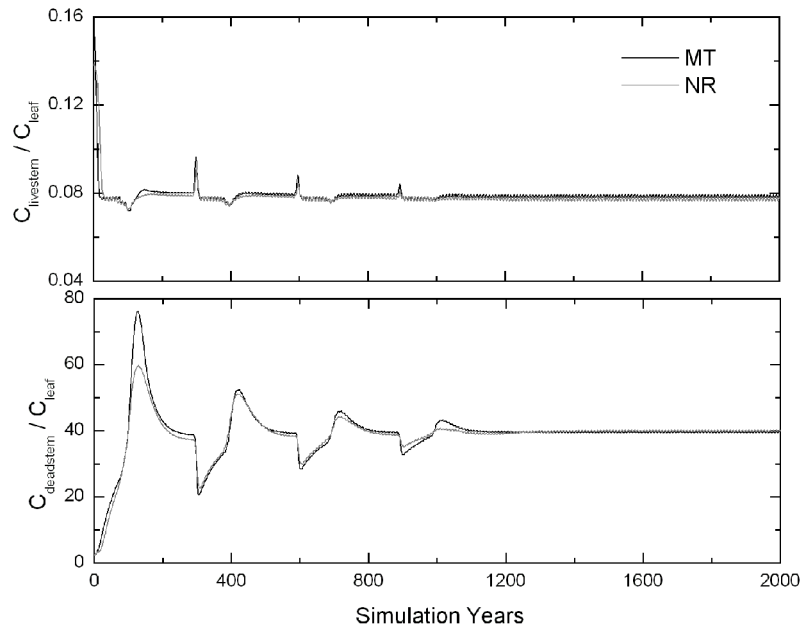


972
973
974
975

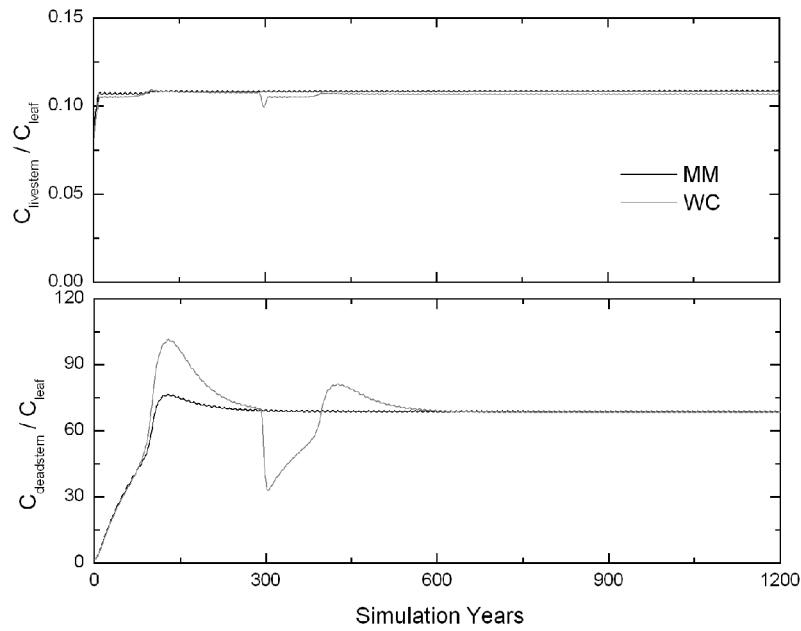
(d) WC

Fig. 3. (Continued).

976



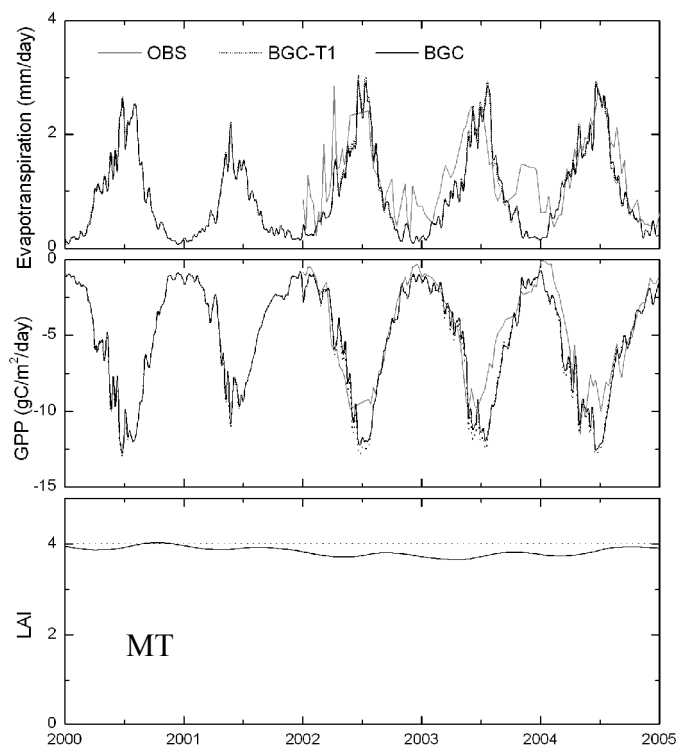
(a) ENF



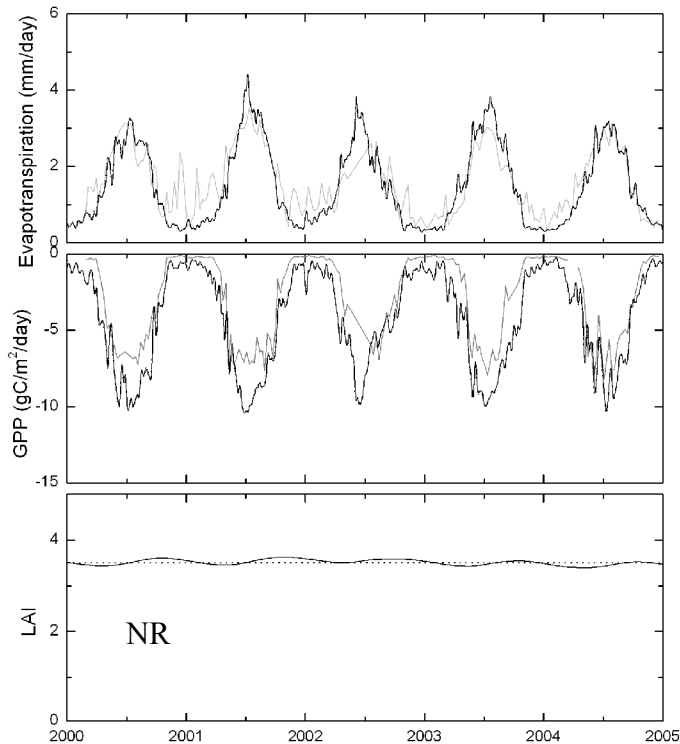
(b) DBF

Fig. 4. Evolutions of biomass ratios in model “spin-up” simulations for (a) Evergreen Needle Forest and (b) Deciduous Broadleaf Forest. The two panels (from top to bottom) show biomass ratios between: (1) live stems and leaves; (2) dead stems and leaves, respectively.

987



988

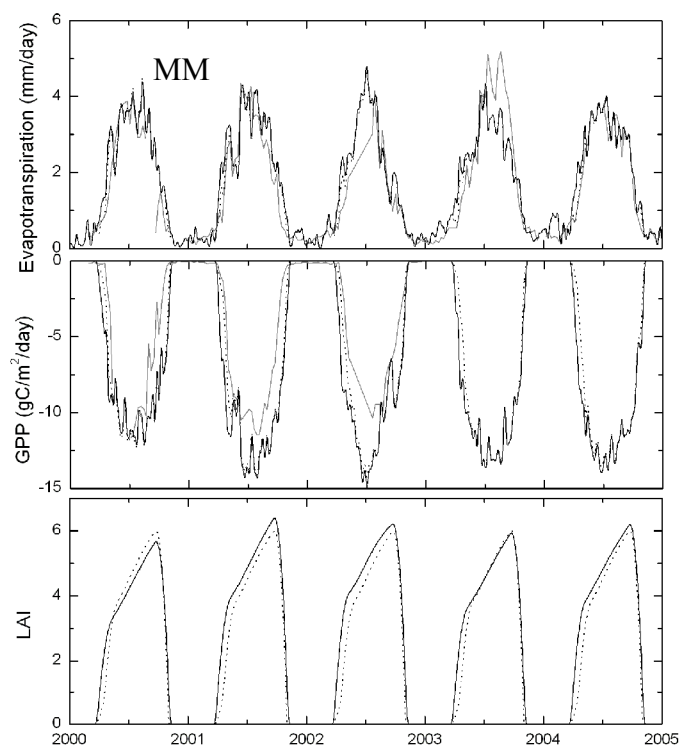


989

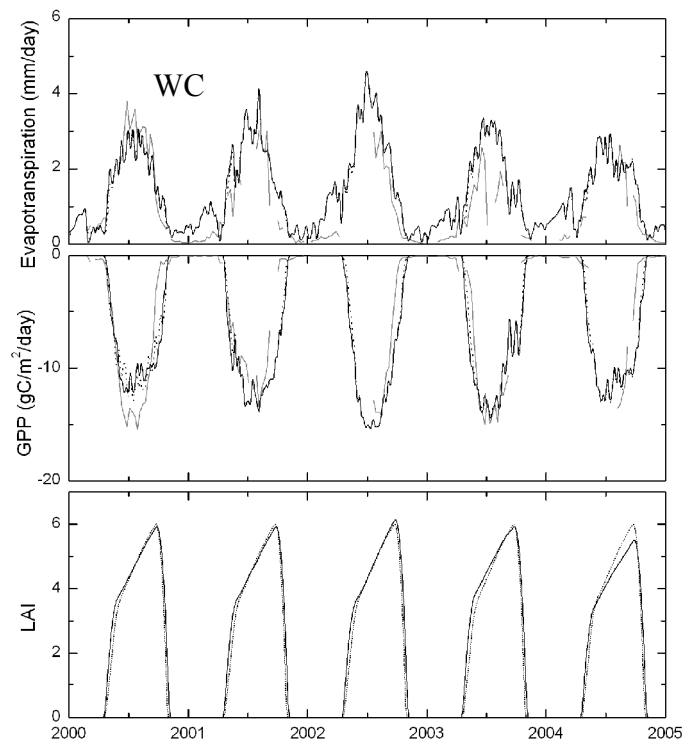
990

991 Fig. 5. ET, GPP, and LAI simulated by the calibrated Biome-BGC model (solid black
 992 lines; “BGC”). Also shown are the corresponding results of the first-tier model (dotted
 993 black lines; “BGC-T1”) and the tower measurements (solid gray lines; “OBS”).

994



995



996

997

998 Fig. 5. (Continued).

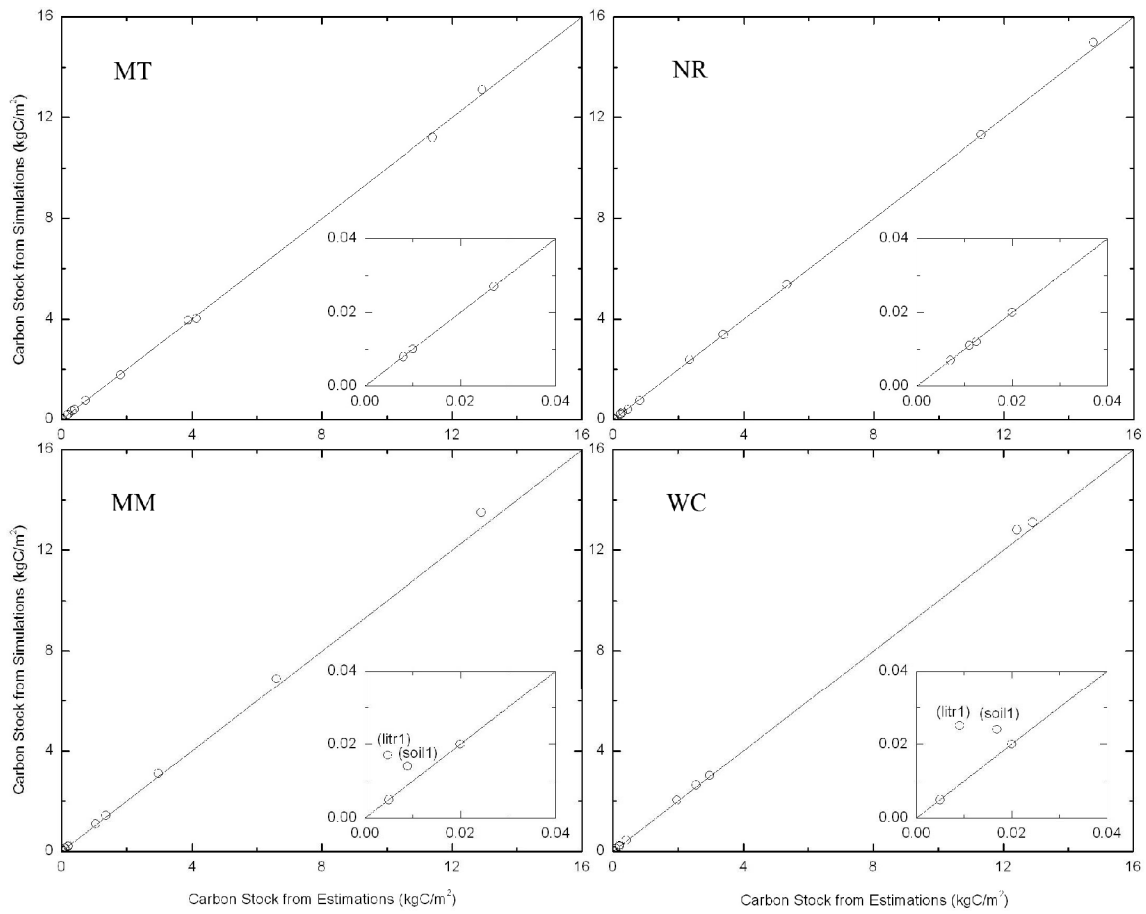


Fig. 6. Comparison between carbon stocks estimated by the hierarchical analysis (of the second- and the third-tier models) and simulated by the calibrated Biome-BGC model.